

# **Carbon Nanotube Linear Bearing Nanoswitches**

**V. V. Deshpande, H.-Y. Chiu, H. W. Ch. Postma, C. Mikó<sup>1</sup>, L. Forró<sup>1</sup>, M. Bockrath**

Department of Applied Physics, California Institute of Technology, Pasadena, CA 91125

<sup>1</sup>IPMC/SB, EPFL, CH-1015 Lausanne-EPFL, Switzerland

**Microelectromechanical structures have produced a wealth of novel devices for sensing, actuation, and lab-on-a-chip applications. Making smaller nanomechanical systems promises faster and more compact versions of their larger counterparts, opening up the possibility of highly-integrated nanoscale machines and logic circuits<sup>1,2</sup>. However, challenges such as friction and precise control of device geometry remain important obstacles to the miniaturization of mechanical systems. Carbon nanotubes promise to address many of these challenges because of their intrinsic nanoscale dimensions, mechanical stiffness, structural perfection, and low inter-shell friction. Here we exploit the remarkable low-friction bearing capabilities<sup>3-5</sup> of multi-walled carbon nanotubes to realize a nanoelectromechanical switch that operates on an entirely different principle than previous efforts exploiting nanotube bending<sup>6-10</sup>. Acting as a non-volatile memory element, our devices are straightforward to implement, self-aligned and do not require complex fabrication or geometries allowing for convenient scalability.**

Our nanotube bearing devices are fabricated in high yield by using electric breakdown<sup>11</sup> to create gaps in a freestanding multi-wall nanotube device producing an insulating OFF state. The devices are actuated with electrostatic forces and undergo linear bearing motion that telescope the inner shells in the two MWNT segments<sup>12</sup> so that they bridge the gap. This restores electrical contact and produces an ON state. Adhesion forces between the nanotube ends maintain the conductive state until an insulating state is controllably restored using a gate voltage, enabling repeated ON/OFF cycles. We thereby create three-terminal non-volatile memory devices. We model the device behavior by

considering the balance of electrostatic forces tending to close the device and restore the conductance and the retraction force from the inter-tube van der Waals forces. A fit of our model to data yields an estimate for the inner shell retraction force, which agree with theoretical calculations as well as the results from atomic force microscopy (AFM) measurements<sup>13</sup>. Our results suggest that the intra-tube electrostatic repulsion makes a significant contribution to actuating the bearing motion. Finally, we estimate the switching speed of our devices, and find sub-nanosecond switching times for the typical nanoscale device geometries employed in our experiment, with considerable scope for further optimization of switching speed by using shorter and thinner nanotubes.

Samples are fabricated by one of two methods on top of heavily doped Si wafers capped by 300 nm of SiO<sub>2</sub>. The first method is to evaporate Cr/Au contacts on arc-discharge synthesized MWNTs (dispersed in 1,2-dichloroethane) deposited on the substrate, and then using 10:1 buffered HF to etch the oxide and suspend the tubes. The second is by forming the electrical leads, etching the oxide with 10:1 buffered HF and then depositing MWNTs on top. A device schematic with the nanotubes on top of the leads is shown in the inset to Fig. 1.

Our ~40 samples studied typically had an initial resistance ranging from ~10 k $\Omega$  to a few M $\Omega$ . A sufficiently high voltage  $V$  across the higher-resistance samples usually resulted in a rapid drop in resistance<sup>14, 15</sup>. This phenomenon enabled us to obtain low-resistance nanotube devices with resistance ~10-20 k $\Omega$  from nearly all contacted nanotubes. Figure 1 shows an  $IV$  curve taken in an Ar atmosphere from a device that was pre-annealed (device D1). The current rises approximately linearly until  $V \sim 4.45$  V at which point  $I$  drops to zero and  $V$  is quickly ramped down. This observation is consistent

with previous work in which heating and electrical stress result in the successive breakdown of the nanotube shells<sup>11</sup>. Indeed, SEM examination of devices after breakdown typically shows two segments with tapering ends, with each segment consisting of 10-30 shells, separated by a gap  $d \sim 5-20$  nm. Figure 1 shows an SEM image from a representative device D2 with such a gap. After the gaps are formed, the devices are in an insulating OFF state, consistent with expected negligible tunnel current for electrode separation exceeding  $\sim 1-2$  nm.

On application of a higher bias (typically in the range  $\sim 5-10$  V) to D1 in the OFF state, at a voltage  $V=4.53$  V as shown in Fig. 2, the current increases abruptly, leading to a conductive ON state (open squares). Once the bias was reduced to 0 V, the device remains latched in this ON state, showing a finite zero-bias resistance (filled squares). In the latched ON state, subsequent SEM imaging of the devices shows that the gap vanishes, indicating nanomechanical motion of the nanotube shells to physically rejoin the two nanotube segments and complete the electrical circuit. The Fig. 2 lower right inset shows this closure for device D2. Our devices thus act as an electrostatically actuated nanomechanical switch.

Careful examination of the MWNT positions in a number of representative samples before and after joining showed that the outer shell remains pinned to the contact even when gaps as large as  $\sim 20$  nm have been closed. Furthermore, SEM examination of our devices rarely shows any observable slack, consistent with the high mechanical stiffness of the  $\sim 10-20$  nm diameter MWNTs. Thus, actuation is unlikely to occur in general by nanotube bending. Having ruled out these possibilities, we then consider telescoping of inner shells from their outer casing as the actuation mechanism<sup>3</sup>. We use

the linear bearing model of Cumings and Zettl<sup>3</sup> to model the van der Waals force between shells within the MWNT. The bearing is expected to act as a constant-force spring, *i.e.* the force is independent of the extended length, with the expected retraction force  $F_R = \alpha R$ , with  $R$  the extended core radius and  $\alpha \sim 1$  N/m a constant. To close the circuit,  $F_R$  must be overcome by the electrostatic force due to the applied voltage. To model the electrostatic force, we approximate the MWNT segments with a cone for the tapered part, and a spherical cap at the tip (Fig. 2 upper left inset)<sup>16</sup>. The geometric parameters for this model (cap radius  $R$ , gap  $d$ , cone half-angle  $\theta$ ) are carefully extracted from the SEM images using a MATLAB image-processing program<sup>17</sup>.

The two main force contributions arise from electrostatic attraction between the segments and intra-shell electrostatic repulsion within a segment. Both of these forces tend to slide one or more shells out to close the gap. It is most straightforward to estimate these for the case where the two segments are far apart ( $d \gg R$ ). In this case, the attractive force between segments (considered to be point charges for this evaluation) is  $\pi\epsilon_0 V^2 R^2 / (d + 2R)^2$  while the repulsive force within a segment (modeled as force between two halves of a charged sphere) is  $\pi\epsilon_0 V^2$ . The force balance gives,

$$\alpha R = \pi\epsilon_0 V^2 \left[ \frac{R^2}{(d + 2R)^2} + 1 \right] \quad (1)$$

Plotting  $V^2$  vs. of  $R$  for data points with  $d/R \gg 1$  should thus yield a straight line with a slope  $\alpha / \pi\epsilon_0$  where  $\alpha \sim 1$  N/m, obtained from previous AFM measurements<sup>13</sup>. Scaling data points as  $d/R$  in Fig 3, indeed we find that data points with the largest  $d/R$  (corresponding to the bigger squares) lie closest to  $\alpha = 1$  N/m.

This demonstrates that for  $d/R$  in this range the dominant actuation force comes from the intra-tube repulsive forces rather than the inter-tube attractive forces. For data with  $d \sim R$  (corresponding to the smaller squares) the data falls below the line, signifying a smaller voltage to overcome the van der Waals forces for a given  $R$ . Although accurate modeling of the electrostatics for  $d \sim R$  is challenging due to lack of charge distribution information on individual shells, we expect that in this regime both the electrostatic intra-tube repulsion and inter-tube attraction are  $\sim \pi \epsilon_0 V^2$ , leading to a smaller closing voltage than in the  $d \gg R$  regime, in qualitative agreement with our observations.

The above procedure of electrical breakdown and closing of gap with bias voltage has been applied to double wall nanotubes (DWNTs) as well. DWNTs were obtained commercially from NanoLab, Inc. and had a typical diameter  $d \sim 3-6$  nm. Using the p-doped Si wafer as a back gate in these samples, we find that for high enough gate voltage devices switch back to OFF state, thus enabling repeated ON-OFF cycles. Fig. 4 shows the time-trace plot of DWNT device D3 (with a pre-breakdown resistance of 100k $\Omega$ ) for two cycles in Ar environment. In the OFF state, on applying a bias voltage the conductance increases abruptly at  $V_{sd}=9$ V leading to the ON state. With  $V_{sd}=10$ mV, at  $V_{gate}=110$ V the device snaps back to the zero conductance (OFF) state. On application of bias voltage, at  $V_{sd}=9$ V the device turns ON again. All the devices tested either became insulating or remained latched in the ON state within 3-4 switching cycles.

We consider the possible explanations for this reversible gate-switching. Previously, a gate voltage has been used to induce the same sign charge and create repulsive electrostatic forces between nanotubes in lateral contact<sup>18</sup>, thereby breaking the contact between two nanotubes. However, in our devices this mechanism is unlikely

because with the tapered geometry the electrostatic forces are unlikely to have any tensile component.

Another possibility is that the gate voltage places a bending stress on the nanotube that acts to break the connection. The electrostatic force (per unit length) on the nanotube due to  $V_g$  is  $F_{el} = \pi \epsilon V_g^2 / \{h[\log(2h/R)]^2\}$ . The maximum bending stress corresponding to  $F_{el}$ , (occurring at the mid-point of the nanotube) is  $\sigma = 4F_{el}L^2 / (3\pi d^3)^{19}$ . This is  $\sim 10^{11}$  Pa for  $V = 110$  V and typical values of  $d$ ,  $L$  and  $h$  ( $d = 5$  nm,  $L = 500$  nm,  $h = 350$  nm). We note that this force greatly exceeds the van der Waals forces between tube-ends, which correspond to a binding stress of  $\sim 10^7$  Pa, using the value for the inter-layer adhesion in graphite. Further evidence for this mechanical switching action comes from that we do not see gate-voltage switching with MWNTs which have much larger diameters and greatly-reduced induced bending stress. Also, the gap-closing OFF-ON transition is not as stable as seen in Fig 4, if the device is imaged in the SEM in the intermediate stage or even just exposed to the ambient atmosphere. This and the large magnitude gate-induced bending stress suggests that the nanotube adhesion results from the formation of one or more covalent bonds between the atoms in the tube ends. However, further experiments are necessary to fully elucidate the adhesion mechanism, for example high-temperature vacuum annealing of the device post-breakdown, to close and cap the ends of the inner nanotube shells<sup>20</sup>. It is expected that the tube ends would then adhere with the smaller van der Waals bonds, and may permit, for example, the realization of microwave-frequency oscillators<sup>21, 22</sup> or charge shuttles.

We also note that the observed switching voltage can likely be reduced by optimization of the geometry such as using thinner nanotubes and decreasing the distance

between the nanotube and the back gate. Using a core mass  $m \sim 2 \times 10^{-19}$  kg corresponding to a nanotube of length 500 nm and core radius 5 nm, an accelerating force  $\sim 5$  nN, and a gap distance  $\sim 5$  nm, we estimate using Newton's laws a switching speed  $\sim 400$  ps, comparable to silicon-based transistor technology. This could be reduced substantially in principle by using shorter core lengths and smaller diameter to decrease  $m$ .

In sum, we report nanoelectromechanical non-volatile memory devices that operate by using multi-walled nanotubes as a low-friction bearings. The devices are straightforward to fabricate in high yield and go through reversible ON-OFF conductance cycles with extremely high estimated switching speeds and high ON/OFF ratios. Aside from using their use as nanoscale memory elements, their unique closing motion can be exploited, for example, as adjustable-gap probes to make electrical contact to other nanostructures that are attached using the flexible chemistry of the open nanotube ends.

## References

1. Roukes, M. Nanoelectromechanical systems face the future. *Phys. World* **14**, 25-31 (2001).
2. Rueckes, T. *et al.* Carbon nanotube-based nonvolatile random access memory for molecular computing. *Science* **289**, 94-97 (2000).
3. Cumings, J. & Zettl, A. Low-friction nanoscale linear bearing realized from multiwall carbon nanotubes. *Science* **289**, 602-604 (2000).
4. Fennimore, A.M. *et al.* Rotational actuators based on carbon nanotubes. *Nature* **424**, 408 (2003).
5. Bournalon, B., Glattli, D.C., Miko, C., Forro, L. & Bachtold, A. Carbon nanotube based bearing for rotational motions. *Nano Lett* **4**, 709 (2004).
6. Kinaret, J.M., Nord, T. & Viefers, S. A carbon-nanotube-based nanorelay. *Appl. Phys. Lett.* **82**, 1287 (2003).
7. Cha, S.N. *et al.* Fabrication of a nanoelectromechanical switch using a suspended carbon nanotube. *Appl. Phys. Lett.* **86**, 083105 (2005).
8. Jang, J.E. *et al.* Nanoelectromechanical switches with vertically aligned carbon nanotubes. *Appl. Phys. Lett.* **87**, 163114 (2005).
9. Dujardin, E., Derycke, V., Goffman, M.F., Lefevre, R. & Bourgoin, J.P. Self-assembled switches based on electroactuated multiwalled nanotubes. *Appl. Phys. Lett.* **87**, 193107 (2005).

10. Lee, S.W. *et al.* A three-terminal carbon nanorelay. *Nano Lett* **4**, 2027-2030 (2004).
11. Collins, P.G., Hersam, M., Arnold, M., Martel, R. & Avouris, P. Current saturation and electrical breakdown in multiwalled carbon nanotubes. *Phys. Rev. Lett.* **86**, 3128 (2001).
12. Forro, L. Nanotechnology - Beyond Gedanken experiments. *Science* **289**, 560-561 (2000).
13. Seiji, A. & Nakayama, Y. Interlayer sliding force of individual multiwall carbon nanotubes. *Jpn. J. Appl. Phys.* **42**, 4830 (2003).
14. Chiu, H.Y. *et al.* Ballistic Phonon Thermal Transport in Multiwalled Carbon Nanotubes. *Phys. Rev. Lett.* **95**, 226101 (2005).
15. Huang, J.Y. *et al.* Atomic-scale imaging of wall-by-wall breakdown and concurrent transport measurements in multiwall carbon nanotubes. *Phys. Rev. Lett.* **94**, 236802 (2005).
16. Hudlet, S., Saint Jean, M., Guthmann, C. & Berger, J. Evaluation of the capacitive force between an atomic force microscopy tip and a metallic surface. *Eur. Phys. J. B* **2**, 5 (1998).
17. We carefully calibrated the SEM radius measurements by comparing SEM images to AFM images on the same nanotube, for a selected subset of the nanotubes. We also note that the radius measurement error is  $\sim\pm 1\text{nm}$  as indicated in Fig. 3
18. Kim, P. & Lieber, C.M. Nanotube Nanotweezers. *Science* **286**, 2148-2150 (1999).
19. Timoshenko, S. *Strength of Materials*. (Krieger Pub. Co., 1983).
20. Geng, H.Z. *et al.* Opening and closing of single-wall carbon nanotubes. *Chem. Phys. Lett.* **399**, 109-113 (2004).
21. Zheng, Q.S. & Jiang, Q. Multiwalled carbon nanotubes as gigahertz oscillators. *Phys. Rev. Lett.* **88**, 045503 (2002).
22. Legoas, S.B. *et al.* Molecular-dynamics simulations of carbon nanotubes as gigahertz oscillators. *Phys. Rev. Lett.* **90**, 055504 (2003).

### Acknowledgements

We thank Alireeza Ghafari for assistance with fabrication. M. B. acknowledges the support of ONR and Arrowhead Research Corporation. The work in Lausanne was supported by the Swiss NSF and its research pool "Nanoscale Science".

Correspondence and requests for materials should be sent to M. B.

**Fig. 1. Relay device from freestanding MWNT.**

Main panel:  $I$ - $V$  characteristics of device D1 leading to electrical breakdown. Upper left inset: MWNT device geometry with attached electrodes and back gate. Lower-right inset: MWNT D2 with nm-size gap after electrical breakdown.

**Fig. 2. Relay device ON characteristics.**

Main panel: Abrupt rise in conductance of device D1 on sweeping of voltage  $V_{sd}$  (open squares) and subsequent latching in the ON state (filled squares). Lower right inset: SEM image of D2 after latching shows that gap has closed. Upper right inset: Schematic cup and cone model of the tube ends used for analysis.

**Fig. 3. Plot of  $V^2$  vs  $R$ .**

Data points' sizes are proportional to  $d/R$ . Plot shows that data matches the parameter-free model (as indicated by the force constant of 1N/m) closely for large  $d/R$ , where it is expected to have the greatest validity. The plot also reveals that samples with nanotube segments close-in ( $R \sim d$ ) are actuated at lower  $V$  than those well separated ( $d \gg R$ ).

**Fig. 4. Three-terminal relay switching and operation**

Plot shows the time trace of bias voltage ( $V$ ), gate voltage ( $V_g$ ) and conductance ( $G$ ) for DWNT device D3 for two cycles. The device initially in OFF state turns ON, OFF and ON again as seen in the plot of  $G$ . Transport data was obtained from D3 in series with a 1 M $\Omega$  protection resistor.

Fig. 1

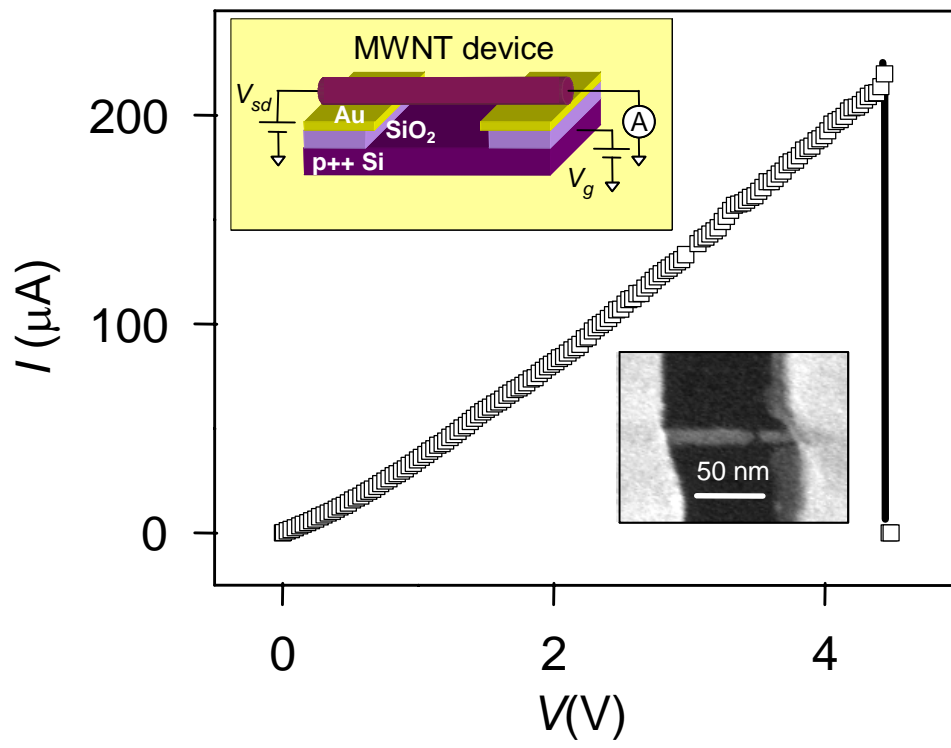


Fig. 2

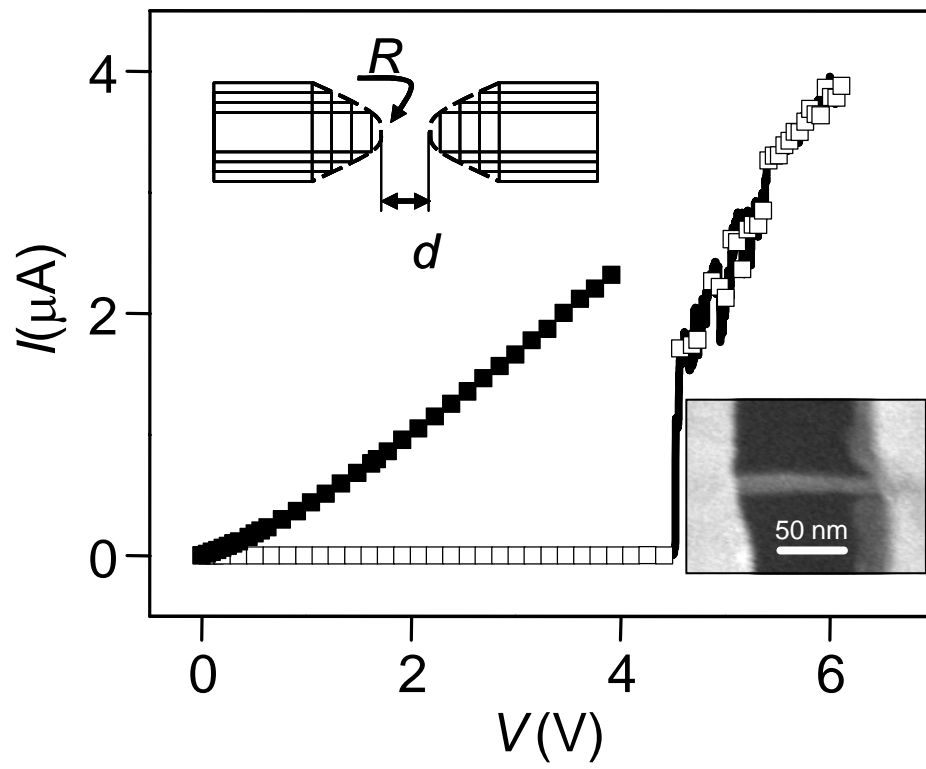


Fig. 3

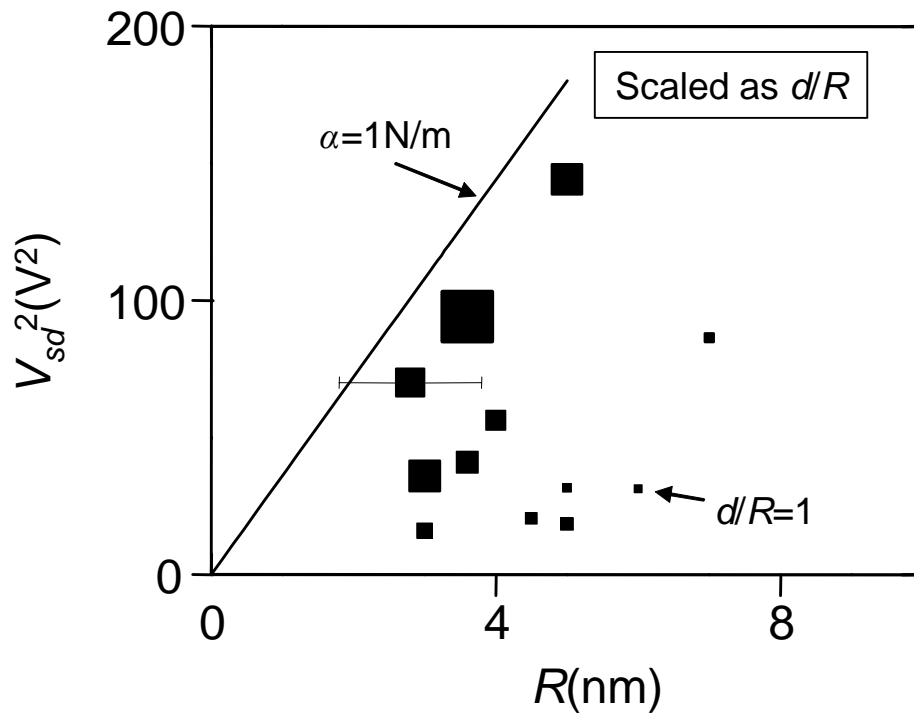


Fig. 4

